

FOUR YEARS OF ASTROMETRIC MEASUREMENTS WITH THE MARK III OPTICAL INTERFEROMETER

C.A. HUMMEL¹, D. MOZURKEWICH², N.M. ELIAS II³,
A. QUIRRENBACH⁴, D.F. BUSCHER¹, J.T. ARMSTRONG¹,
K.J. JOHNSTON³, R.S. SIMON⁵, AND D.J. HUTTER³

NRL/USNO Optical Interferometer Project

U.S. Naval Observatory, 3450 Massachusetts Avenue NW, Washington, DC 20392

Electronic mail: chummel@atlas.usno.navy.mil, mozurk@rira.nrl.navy.mil,
nme@fornax.usno.navy.mil, quirrenbach@mpei3@mpens.mpe-garching.mpg.de,
dbuscher@atlas.usno.navy.mil, tarmstr@atlas.usno.navy.mil, ken@spica.usno.navy.mil,
rsimon@nrao.edu, dhutter@atlas.usno.navy.mil

¹Universities Space Research Association, 300 D Street SW, Suite 801, Washington, DC 20024

²Naval Research Laboratory, Remote Sensing Division, Code 7210, Washington, DC 20375

³U.S. Naval Observatory, 3450 Massachusetts Avenue NW, Washington, DC 20392

⁴Max-Planck-Institut für Extraterrestrische Physik, Giessenbachstr., 85748 Garching, Germany

⁵NRAO, Edgemont Road, Charlottesville, VA 22903

ABSTRACT

Repeated measurements of the eleven FK5 stars selected by Shao *et al.* (1990, AJ, 100, 1701) were performed with the north-south and east-south astrometric baselines of the Mark III optical interferometer in order to estimate the accuracy of wide-angle astrometry. Even though the declination range of these stars is insufficient to determine absolute declinations, we were able to determine corrections to the FK5 positions at four epochs with an accuracy of about 13 milliarcseconds (mas) in declination and 23 mas in right ascension. Measurements at two different wavelengths were used to correct for refractive index fluctuations in the turbulent atmosphere. The pathlength difference between the two arms of the interferometer was monitored during the night with an internal white-light interferometer. The accuracy of the positions is limited by systematic errors due to unmonitored changes in the baseline coordinates and due to low-frequency water vapor fluctuations. However, these results demonstrate the potential of future optical interferometers for the measurement of stellar positions with mas accuracy.

1. INTRODUCTION

The capability of the Mark III optical interferometer⁶ of measuring stellar positions over wide angles has been demonstrated by Mozurkewich *et al.* (1988, henceforth M88), and the precision of such measurements shown by Shao *et al.* (1990, henceforth S90) to exceed today’s standard of the FK5 catalog. These authors, however, expressed the need for repeated observations in order to ascertain the accuracy that can be achieved with a long-baseline astrometric interferometer. This “proof of concept” is important for the Astrometric Optical Interferometer (AOI), which is a sub-array of the Navy Prototype Optical Interferometer currently under construction at Lowell Observatory, Arizona, in a collaboration between the U.S. Naval Observatory and the Naval Research Laboratory (e.g. Weiler *et al.* 1992, Hutter 1993). The AOI is expected to measure relative stellar positions with an accuracy of a few milliarcseconds (mas). By measuring the proper motions of the stars it will be able to maintain the catalog established by the HIPPARCOS astrometry satellite (HIPPARCOS positions will have an internal accuracy of about 2 mas; Perryman 1990). With instruments like HIPPARCOS and AOI, optical astrometry is about to achieve a level of precision far greater than classical meridian circle measurements, which are believed to be internally consistent at ≈ 50 mas (e.g. FK5 catalog; Fricke *et al.* 1988).

2. WIDE-ANGLE ASTROMETRY WITH THE MARK III INTERFEROMETER

The Mark III optical interferometer was described by Shao *et al.* (1988), and the fundamentals of wide-angle astrometry with this instrument were discussed by M88 and

⁶The Mark III optical interferometer, located on Mt. Wilson near Los Angeles, California, is operated by the Remote Sensing Division of the Naval Research Laboratory (NRL) with funding from the Office of Naval Research.

S90. The Mark III features two astrometric baselines oriented north-south and east-south, $\mathbf{B}_{N-S} = (6.753 \text{ m}, 0.032 \text{ m}, -9.925 \text{ m})$ and $\mathbf{B}_{E-S} = (3.669 \text{ m}, -10.061 \text{ m}, -5.398 \text{ m})$, respectively, in a right-handed coordinate system, with Z axis parallel to the Earth’s axis, and Y axis toward the east point on the horizon. Only one baseline may be used at a time. The siderostats are mounted on massive concrete piers located in protective huts. A stellar interference pattern (“fringes”) is produced by combining the two beams from each siderostat at a beamsplitter (Michelson interferometer). Optical delay lines, monitored by laser-interferometers, are used to compensate for the geometrical delay. Piezo-activated mirrors track the rapid motion of the fringe pattern in a wide-band channel (650 nm – 900 nm) so that precise measurements of the delays can be obtained as the stars move across the sky. The fundamental equation relating delays and star positions is

$$d_i(t) = \mathbf{B} \cdot \mathbf{S}_i(t) + C(t), \tag{1}$$

with the baseline vector $\mathbf{B} \equiv (B_x, B_y, B_z)$, the unit vector \mathbf{S} to star i at time t and the delay “offset” $C(t) = C_0 + \Delta C(t)$, i.e. the pathlength difference between the arms of the interferometer at time t . We note that the delay lines are placed in evacuated tanks so that atmospheric refraction does not affect the measured delays in the approximation of a plane-parallel atmosphere. A time dependence of the baseline coordinates is not included in the equation, since they cannot be measured with the Mark III; drifts at the micron level due to thermal variations *are* noticeable in the delay data and manifest themselves as systematic errors.

Since the actual baseline coordinates are not known *a priori* with sufficient accuracy, they have to be determined simultaneously with the star positions from the delay data.

Expanding Eq. (1) gives

$$d_i(t) = C_0 + B_z \sin \delta_i - B_y \cos \delta_i \sin h_i(t) + B_x \cos \delta_i \cos h_i(t), \quad (2)$$

where t is the local sidereal time, $h_i(t) \equiv t - \alpha_i$ is the instantaneous hour angle, α_i is the right ascension, and δ_i the declination of star i . The time dependence of C is measured by an internal white-light interferometer (see Sec. 3) and applied to the data, so that $C(t)$ can be replaced by C_0 . The declinations are assumed to be with respect to the instantaneous celestial pole (but see Sec. 5); a zero point for the right ascensions cannot be determined from these observations and is therefore set arbitrarily. Expanding Eq. (2) in terms of assumed baseline components and star positions plus small offsets gives (dropping index i for convenience)

$$d_{\text{res}}(t) \equiv d(t, \delta + \Delta\delta, \alpha + \Delta\alpha, \mathbf{B} + \Delta\mathbf{B}) - d(t, \delta, \alpha, \mathbf{B}) = X \cos h(t) - Y \sin h(t) + Z \quad (3)$$

where

$$\begin{aligned} X &= \Delta B_x \cos \delta - \Delta\delta B_x \sin \delta + \Delta\alpha B_y \cos \delta \\ Y &= \Delta B_y \cos \delta - \Delta\delta B_y \sin \delta - \Delta\alpha B_x \cos \delta \\ Z &= \Delta B_z \sin \delta + \Delta\delta B_z \cos \delta + \Delta C_0. \end{aligned}$$

Measurements of residual delays $d_{\text{res}}(t)$ for a star i over a range of hour angles provide estimates for X_i , Y_i , and Z_i . For an ensemble of at least three stars at different declinations all the unknown parameters can be solved for simultaneously (i.e. baseline and star position offsets: the “solution vector”). However, for the set of stars selected by S90, the usefulness of this “global” solution is limited because of the insufficient declination range of the stars. This situation is a two-dimensional degeneracy of the astrometric solution. The degeneracy

in right ascension is complete and inherent to all measurements which do not determine the location of the equinox at the same time. Thus, a multiple of an “eigenvector,” with the right ascension elements set to one and the declination elements set to zero, can be added to the solution vector without changing the quality of the fit. We chose to set the mean right ascension offset to zero. As for the declinations of the selected FK5 stars, the design matrix (3) becomes nearly singular, with the right ascension elements of the eigenvector equal to zero and the declination elements approximately proportional to $1/\tan \delta_i$. (If this second eigenvector had declination elements equal to one instead, we would do true relative astrometry in both dimensions.) From the solutions consistent with the data, we select the vector with the smallest length, i.e. the solution with the smallest “distance” to the initial estimates (“principal solution”). We use the singular value decomposition method as described by Press *et al.* (1986) for the linear least-squares fit of the parameters to the delay data. As an example, Fig. 1 plots the declination elements of an eigenvector (August 1992) and actual offsets determined by a *global* solution. The latter provided an equally good fit to the data as the principal solution, even though the actual offsets were of the order of arcseconds.

Initial estimates for the star positions are derived from their FK5 positions. These are also used to determine the initial estimates for the baseline coordinates of each night. Apparent places for the FK5 stars at the epoch of observation were calculated from their mean place at Epoch J2000.0 (Fricke *et al.* 1988), using the U.S. Naval Observatory subroutine package NOVAS (Kaplan *et al.* 1989). NOVAS accounts for precession, nutation, proper motions, and parallaxes (taken from the General Catalogue of Trigonometric Stellar Parallaxes, Jenkins 1952) and conforms to the IAU convention for coordinate transformations.

An alternative method chosen by M88 and S90, the “two-step” procedure, fits the

baseline coordinates to the delay data first, assuming apparent FK5 positions for the stars (Step 1). Using these baseline coordinates, fit residuals are then modeled by “residual positions” which update the initial positions (Step 2). This procedure is iterated twice. However, the solution of this procedure is susceptible to the specific hour angle coverage of the stars at that epoch, and to systematic biases in the FK5. As the authors of S90 point out, the two-step procedure is useful for demonstrating the precision of the interferometric measurements; it is not suited to determine true star positions. Instead, the repeatability of the derived residual positions would only reflect the repeatability of the baseline solution to give the same FK5 offsets. We will make use of this method only to demonstrate internal consistency of a small set of data taken in August 1992 (see Sec. 5); other results correspond to the principal solution as described in the previous paragraphs.

3. DISCUSSION OF MEASUREMENTS AND DATA REDUCTION

Two major improvements in precision over results reported by M88 were achieved by S90 by implementing delay offset metrology to reduce residual delay trends which often correlate with changes in the delay offset C , and a “two-color” method to correct for low-frequency delay variations caused by refractive index fluctuations in the turbulent atmosphere. In the first method, an internal white light beam, directed towards one “exit” of the beamsplitter, travels backwards to corner cubes attached to the back of the movable siderostat mirrors. The position of the fringe pattern produced from the return beams is monitored throughout the night. However, the effectiveness of the method is limited because none of the other parameters of the baseline are measured. If, for example, the inclination of the N-S baseline changes, the delay offset might not change at all but the measured delays will exhibit systematic variations, mimicking those caused by nonzero residual positions.

3.1 The Two-Color Method

The success of the two-color method (Colavita *et al.* 1987) is based on the fact that the dominant cause for optical refractive index fluctuations are temperature and pressure fluctuations. The refractive index of air can be written

$$n(\lambda, P, T, e) = A(\lambda)\frac{P}{T} - B(\lambda)\frac{e}{T} + 1,$$

where P is the total pressure in mb, e is the partial pressure of water vapor in mb, T is the temperature in K, and A and B are the dispersion relations (Owens 1967). With the Mark III interferometer tracking fringes in the wide-band channel, we coherently average the phase (“one-color” delays) for 200 ms in three narrow channels centered at λ 800 nm, 550 nm, and 500 nm, with 22 nm, 25 nm, and 40 nm bandwidth, respectively. (Small bandwidths are used to minimize the effects of residual instrumental dispersion.) An estimate for the value of vacuum delay d is given by the “two-color” delay d_{2C} ,

$$d_{2C} \equiv d_{\text{red}} - D(d_{\text{blue}} - d_{\text{red}}),$$

where we defined the dispersion constant $D = (n_{\text{red}} - 1)/(n_{\text{blue}} - n_{\text{red}})$. For dry air, D is independent of pressure and temperature. Two two-color estimates are derived from channel combinations 550/800 and 500/800, for which dry air dispersions constants of $D \approx 100$ and $D \approx 71$, respectively, are adopted. In Fig. 2, two-color delays exhibit significantly reduced low-frequency variations relative to the one-color delay in the tracking channel. Due to the small bandwidths and the large dispersion constants, however, photon noise in the two-color delays is much larger compared to noise in the one-color delay. The uncertainty of a phase measurement due to photon noise is given by (Colavita 1985)

$$\sigma_\phi = \frac{\lambda}{\sqrt{16NV^2}} \text{ microns},$$

where N is the number of photons per (coherent) integration time, and V^2 is the squared visibility. For the scan shown in Fig. 2 (FK5 1568), $N_{\text{red}} = 475$, $N_{\text{green}} = 205$, $N_{\text{blue}} = 280$,

$V_{\text{red}}^2 = 0.41$, $V_{\text{green}}^2 = 0.28$, and $V_{\text{blue}}^2 = 0.33$, so that $\sigma_\phi = 0.014$, 0.018 , and 0.013 microns for the three channels, respectively. The uncertainty of a two-color delay measurement is given by

$$\sigma_{2C} = D\sqrt{\sigma_{\phi_1}^2 + \sigma_{\phi_2}^2} \text{ microns.}$$

For the scan shown in Fig. 2, we derive $\sigma_{2C} = 2.3$ microns and $\sigma_{2C} = 1.4$ microns for the channel combinations 550/800 and 500/800, respectively. These values come close to the actual rms variation of the two-color delays of about 2.7 microns and 1.6 microns, respectively. The rms variation of the one-color delay in the tracking channel is 3.3 microns, and is entirely dominated by low-frequency variations.

We averaged the two-color data points over the length of a scan and used the rms variation of the 200 ms coherent averages as uncertainty estimate for the scan-average. As we shall see, there are significant systematic errors in the delays (baseline drifts, water vapor fluctuations, and possibly other effects), so that this procedure seemed appropriate when longer integration times would not actually improve the accuracy of the measured delays. A weighted mean was calculated from the channel combinations 550/800 and 500/800. The typical precision of the averaged two-color delays is about 1.8 microns. (a 1 micron delay offset corresponds to a 17 mas positional offset on the sky on a 12 m baseline.) In Fig. 3 we plot the two-color delay differences (omitting uncertainties) between the two channel combinations. The observed scatter is consistent with photon noise. The mean difference is offset from zero due to residual internal dispersion; this offset changes only very slightly (less than one micron) from night to night (due to aperture changes, temperature changes of optical components, etc.) and has no implication for the actual astrometry. We use two-color delay difference plots to edit bad data points. From Fig. 4, which plots the delay residuals from star position fits versus the zenith angle, we conclude that the two-color method appears to be free of systematic errors at a level of at least ≈ 1 micron over a large

range of zenith angles. Since the measurement of stellar positions requires observation of stars over as wide a declination range as possible, the performance of the two-color method at large zenith angles might be a fundamental limitation of the interferometer technique.

3.2 *The Identification of Fringes*

Since phase differences are used to calculate delay differences in the two-color method, it is necessary to determine which fringe order was tracked for each data point. Due to the large bandwidth of the fringe tracker channel, the interference pattern in this channel consists of only 5 fringes (orders -2 , -1 , 0 , $+1$, and $+2$). The visibility of the central (0^{th} -order) fringe is considerably higher than the visibility of the other orders. By specifying a visibility threshold during the observations, the fringe tracker is enabled to “recognize” and “lock” onto the central fringe. Only central fringe data are used, the fraction of which may get small if seeing conditions deteriorate.

In order to identify the fringes in a scan, we plot the delay differences of the channel combinations 550/800, 500/800, and 700/800 versus the residual one-color delay (see Figs. 5 a–c). The data points spread out along fairly well defined bands corresponding to the different fringes (the scatter depends on seeing conditions, stellar brightness, and coherent pre-integration time). Due to the large wavelength separation of the first two wavelength combinations, the bands wrap around. For example, the second-order fringe is located at almost the same position as the central fringe. The identification scheme works as follows: we project all data points onto the axis of zero delay difference using the value of the dispersion (the inverse slope of the bands), and calculate histograms to determine the exact positions and widths of the bands. Data points of the central band in the first channel combination are separated into orders -2 , 0 , and $+2$ using their position in the third combination (due to the small wavelength separation, the different orders do not wrap around). All the remaining points (which must be of order $+1$ or -1) are then separated

again using the third channel combination. The second channel combination is used as a further check on the identification, as well as the visibility amplitude measured in the wide-band channel, which must be highest for the central fringe data points and lowest for points of order +2 and –2 (see Fig. 5 d).

3.3 Water Vapor Fluctuations

As Colavita *et al.* (1987) have pointed out, water vapor fluctuations pose a fundamental limit to the two-color method. This is because the dispersion relation $B(\lambda)$ is different from the dry air dispersion relation $A(\lambda)$. (For pure water vapor, $D = B_{\text{red}}/(B_{\text{blue}} - B_{\text{red}}) \approx -66$, and -48 for the two channel combinations). We note that a three-color method would be able to correct for low-frequency variations in temperature, pressure, and water vapor, using

$$d_{3C} = \frac{d_{\text{red}}X_{\text{red}} + d_{\text{green}}X_{\text{green}} + d_{\text{blue}}X_{\text{blue}}}{X_{\text{red}} + X_{\text{green}} + X_{\text{blue}}},$$

where

$$\begin{aligned} X_{\text{red}} &= A_{\text{green}}B_{\text{blue}} - A_{\text{blue}}B_{\text{green}} \\ X_{\text{green}} &= A_{\text{blue}}B_{\text{red}} - A_{\text{red}}B_{\text{blue}} \\ X_{\text{blue}} &= A_{\text{red}}B_{\text{green}} - A_{\text{green}}B_{\text{red}}. \end{aligned}$$

(The coefficients are obtained by cyclic permutation of the three colors.) However, with all three colors in the optical region, photon noise in this estimator is increased by a factor of about 3000 over the noise in the one-color delays.

Water vapor fluctuations were the probable cause for the low-frequency intra-scan variations of the two-color delays shown in Fig. 6. The scan was recorded in the last night

of a session on the N-S baseline, lasting from August 7 to 9, 1992. Inspection of other scans of this night shows that they exhibited similar low-frequency residuals. In fact, the median intra-scan rms variation of the two-color delays was ≈ 4.0 and 3.0 microns for the two channel combinations, respectively, compared to ≈ 3.5 and 2.3 microns, respectively, on the previous two nights. (The rms variation in the one-color delay in the tracking channel was ≈ 3.0 microns in all three nights.) Since the dispersion constant for water vapor fluctuations, as mentioned above, is somewhat smaller in magnitude and of opposite sign compared to the dry air dispersion, weak fluctuations tend to decrease the average dispersion, i.e., increase the slope of the bands shown in Fig. 5. We therefore fitted dispersion constants to the central fringe data of each scan of the three nights and found that their respective distributions on August 9 were significantly broader and shifted towards smaller dispersion values, compared to the distributions of the two previous nights (see Fig. 7). This result supports the interpretation of the low-frequency residuals in the two-color delays as being due to water vapor fluctuations.

The occurrence of low-frequency two-color delay intra-scan residuals on August 9 coincided with enhanced scatter of the residual delays (see Fig. 10 and Sec. 5). Since these fluctuations, as we shall see, might have affected a significant fraction of the data obtained with the Mark III interferometer, we will describe in the following the relevant circumstances of this event in more detail. These three nights were very similar in many other respects. All nights were clear (mid-level clouds rolled in on August 11), the relative humidity was at $32\% \pm 4\%$, temperature at $64^\circ \pm 4^\circ\text{F}$, pressure at 857 ± 1 mbar, and moderate winds of about 5 knots prevailed mainly from the SW (W–SW–SE). Seeing conditions were good in all three nights. The median fraction of time the Mark III interferometer tracked the central fringe was similar in all three nights, too. We conclude that the characteristics of water vapor fluctuations can change without simultaneous changes in meteorological conditions so as to become responsible for a significant fraction of the optical seeing (see Masson 1993).

The average actual improvement in precision achieved by the two-color method is demonstrated in Fig. 8 which includes all delay measurements made with the Mark III in the astrometry program since 1988. The tail towards large rms-uncertainties in the one-color delays in the tracking channel (only central fringe data are shown) is absent in the histograms of the two-color delays, and indicates that, in general, the two-color correction has improved the data quality.

4. SUMMARY OF OBSERVATIONS

Table 1 lists the stars observed, together with information regarding parallaxes π , and centennial proper motions μ and μ' , in right ascension and declination, respectively. The selection of the stars for this work represented a compromise between minimum slewing times between stars (a sufficient number of scans per star is important), moderate zenith angles (seeing at large zenith distances is usually poor, and there are limitations to the two-color method at larger zenith angles which are discussed by Colavita *et al.* 1987), minimal obstruction from the siderostat huts, and pointing limitations due to the pipes of a siderostat laser monitoring system (which was removed in 1989). Since the first epoch of August/September 1988 (S90), the same list of stars was observed in October 1988, July 1989, September 1990, September 1991, and August, September, and October 1992. (Observations of different lists were done in parallel, but with limited success.) Table 2 lists the observations, which were used for this work. Data of other epochs were either insufficient or of low quality (see below).

In general, the observations suffered from several problems. First, there are signal strength variations in the delay line laser metrology system related to misalignment of the lasers and dropouts due to excessive vibrations caused by shutters on the beam combination table. These cause the metrology fringe counter occasionally to loose fringe counts (“delay line jumps”) on the order of several tens to hundreds of microns (July 1989, the E-S

baselines in September 1990). Even though these glitches show up in the white light fringe position and can be removed from the delay data, the measurement time (≈ 4 min) prohibits taking more than about 20 white light measurements per night.

Second, the fraction of time the fringe tracker locks onto the stellar central fringe decreases rapidly with deteriorating seeing conditions, thus diminishing the amount of usable data and complicating the central fringe identification.

Third, temperature-related drifts of the baseline vector occasionally would render the delay data uncorrectable by the white light measurements alone, and therefore led to the exclusion of the data from further analysis (October 1992). These drifts cause residual delay trends at a level of up to 10 microns and often happen together with large changes in the white light fringe position (5 to 15 microns peak to peak). This indicates that, in addition to drifts in the beam combiner optics, the causes are in fact drifts of the siderostats. We tried to minimize siderostat temperature variations by controlling the air temperature in the siderostat huts during the day. Unfortunately, due to imperfections in the white light interferometer, white light fringe positions also did not always appear to provide a reliable way to monitor the variations in the delay offset C (i.e., applying the correction would *introduce* residual delay variations.)

Fourth, mechanical imperfections of the siderostat mounts might have introduced delay errors. If the axes of the siderostats do not intersect and are offset from the mirror surface, errors in the delays will occur and correlate with hour angle. As M88 pointed out, this pivot-point offset approximately mimics a change in the baseline coordinates and therefore can be partly removed. We show in Fig. 9 that there is such a correlation of the residual delays with hour angle in the data of August 1992. Data of earlier epochs did not exhibit this effect, indicating a deterioration of the siderostat mechanics and mirror cell alignment over the years. We also note that in *all* nights, the scatter of the two-color delays

is significantly larger than the uncertainty of the weighted scan averages. Aside from water vapor fluctuations (see Sec. 5 and Fig. 10c), Colavita *et al.* (1987) have discussed other effects which could introduce systematic errors into the two-color delays. None of these effects, however, seems to be able to explain the magnitude of the observed variations. Ball bearing errors might be partly responsible. (Recall that therefore we use the rms variation of the 200 ms coherent averages as uncertainty estimate of the scan-averaged two-color delays; see Sec. 3).

5. ASTROMETRIC RESULTS AND DISCUSSION

Stellar position offsets manifest themselves in residual delay variations (Eq. 3). As an example for the repeatability of delay variations measured with the Mark III, we present in Fig. 10 data from three consecutive nights on the N-S baseline from August 1992. Baseline coordinates have been fitted to the delay data for all stars, assuming apparent FK5 positions as initial estimates for the star positions. The delay data for the star FK5 835 (π^2 Pegasi) are plotted with formal uncertainties. The delays consistently show an offset from zero of about four microns, indicative of a declination offset of this star of about 70 mas (solid line in Fig. 10). Two-color delays from the last night (9 August) show increased scatter, which might be related to water vapor fluctuations (see Sec. 3 and Figs. 6 and 7).

In order to get an idea of the star position uncertainty corresponding to the measurement uncertainty of the delay variation, we used the two-step procedure to determine residual positions from each of the three nights. (Since star position fitting is a separate step in this procedure, the uncertainty in the baseline coordinates is not included in the uncertainty of the star positions. Therefore, this method gives a correct estimate of the stellar position uncertainties in the limit that the baselines were determined with high precision by observation of a large number of stars over a sufficiently large declination range. In every other case where the global solution is used to determine both the baseline

coordinates and the star positions, uncertainties in the latter will be larger.) The result, shown in Fig. 11, is that the residual positions have formal uncertainties (derived from the covariance matrix) between 5 mas and 15 mas in declination. (Since the N-S baseline is much less sensitive to right ascension offsets, we do not give results for this coordinate.) In Fig. 12, we present histograms of the formal uncertainties and the normalized deviations (we call the latter the “error distribution” and will make use of this kind of histogram again later). The normalized deviations (“errors”) are deviations of individual positions of a star from the weighted average position of several epochs, divided by the formal uncertainty of the individual position. Since the error distribution in Fig. 12 is nearly Gaussian with unity width, we conclude that the formal uncertainties of the positions are a good estimate for the accuracy.

While the results shown in Figs. 10–12 represent the best achieved with the Mark III in terms of internal consistency (despite the problems of the August 1992 data documented in Fig. 9), the data of the other epochs are of somewhat lesser quality. We have used the principal solution as described in Sec. 2 to derive star position offsets for each epoch. All the data from an epoch were used in a simultaneous fit of star positions and baseline coordinates after initial estimates had been derived as described in Sec. 2. We used the delay uncertainties to weight the data. The reduced χ^2 of the combined baseline and stellar position fits to the data is in the range from 0.7 to 1.3. Figure 13 shows the resulting stellar positions and Fig. 14 the weighted average positions. Since the instantaneous rotational pole for the Mark III may deviate from the celestial pole due to baseline drifts during the night, the zero point of our declinations is somewhat arbitrary and we therefore set the mean declination offset in each epoch to zero (if the baseline coordinates were tied to the local crust via a metrology system, declination measurements would be “absolute”; see Kaplan 1990).

The uncertainties of the stellar positions plotted in Fig. 13 have been scaled so that the error distributions for the right ascension and declination offsets (Fig. 15) effectively were normalized to Gaussians of unity width. The ratio of the mean uncertainty in the right ascensions (≈ 23 mas) to the declinations (≈ 13 mas) is about the same as obtained by S90 (the N-S baseline is mostly sensitive to declination offsets, while the E-S baseline is more sensitive to right ascension offsets, though not as much as an east-west baseline would be). Table 3 lists the results by star and epoch. Entries for epochs are in chronological order (see Table 2). We also give the mean and rms of the delay residuals in the principal solution (cols. 4 and 5).

We note that some of the stars are consistently and significantly displaced from the apparent FK5 positions, indicating that our measurement precision is sufficiently high to reveal intrinsic errors in the FK5 system. The discrepancies are most likely due to errors in the FK5 positions and/or proper motions and/or parallaxes. The accuracy of our measurements and the limited time base are not sufficient to improve the proper motion estimates of the FK5, which have a mean accuracy of about 70 mas/100 y. The large scatter in the individual positions of the star FK5 66 is because this star is a spectroscopic binary (Pan *et al.* 1990). Thus, the relative phase between channels for use in the two-color method contains a nonzero time-variable contribution from the binary model (which we did not attempt to correct). In addition, the variable visibility affects the performance of the fringe tracker in selecting the central fringe, decreasing the amount of usable data. Systematic errors in our data must be responsible for the large scatter or outliers in the positions for stars FK5 1568, 1534, and 52.

6. CONCLUSIONS

We have demonstrated that astrometric measurements with the Mark III optical interferometer have the potential of measuring stellar positions with an accuracy that

exceeds the average FK5 accuracy by more than a factor of two. For some of the selected stars (notably FK5 1619, 862, 79, 848, and 835) we have determined positional offsets from the apparent FK5 position on the order of a few tens of a milliarcsecond.

Due to the small declination range of the stars we could not completely constrain the solution for the declination offsets. In addition, due to the lack of a metrology system to define the instantaneous pole of rotation with respect to the celestial pole in each night, our declinations are not absolute and might be prone to systematic errors.

Systematic errors in the data have limited the accuracy. They appear to be largely due to unmonitored baseline drifts and mechanical imperfections of the siderostats. In addition, water vapor fluctuations have been identified as the probable cause for further systematic errors.

The results demonstrate the potential of optical interferometers with improved design to derive stellar positions with an accuracy easily exceeding the accuracy achievable with classical methods. Instrument stability is the key issue when constructing an astrometric interferometer. It must include a full metrology system in order to monitor changes in the baseline coordinates, additional metrology to tie the array to the local crust of Earth in order to allow the determination of absolute declinations, real time central fringe identification to maximize the amount of useful data, and a sufficiently large sky coverage to eliminate the degeneracy in the declination solutions. The design of the AOI, a prototype of the next-generation astrometric optical interferometers, employs these techniques towards stellar position measurements with an accuracy that should match that of the HIPPARCOS satellite.

We would like to thank Craig Denison and Lu Rarogiewicz for substantial help with the observations, and John Pohlman for helping with the instrument maintenance. A.Q. is

supported by the Alexander von Humboldt Foundation through a Feodor Lynen fellowship.

This work was supported by the Office of Naval Research.

References

- Colavita, M. M. 1985, Ph.D. Thesis, M.I.T., Cambridge, Massachusetts
- Colavita, M. M., Shao, M., & Staelin, D. H. 1987, *Appl. Opt.*, 26, 4113
- Fricke, W., Schwan, H., Lederle, T., Bastian, U., Bien, R., Burkhardt, G., du Mont, B.,
Hering, R., Jährling, R., Jahrei, H., Rser, S., Schwerdtfeger, H. M.,
& Walter, H. G. 1988, *Fifth Fundamental Catalogue*
(Verffentlichungen Astronomisches Rechen-Institut No. 32, Heidelberg)
- Hutter, D. J. *et al.* 1993, in *IAU Symp. No. 158* (in press)
- Jenkins, L. F. 1952, *General Catalogue of Trigonometric Stellar Parallaxes*
(Yale University Observatory, New Haven)
- Kaplan, G. H. 1990, in *Inertial Coordinate System on the Sky*, *IAU Symp. No. 141*,
edited by J. H. Lieske and V. K. Abalakin (Kluwer, Dordrecht), p. 241
- Kaplan, G. H., Hughes, J.A., Seidelmann, P.K., Smith, C.A., & Yallop, B.D. 1989, *AJ*, 97, 1197
- Masson, C. R. 1993, in *IAU Symp. No. 158* (in press)
- Mozurkewich, D., Hutter, D. J., Johnston, K. J., Simon, R. S., Shao, M., Colavita, M. M.,
Staelin, D. H., Hines, B., Hershey, J. L., Hughes, J. A., & Kaplan, G. H. 1988,
AJ, 95, 1269 (M88)
- Owens, J. C. 1967, *Appl. Opt.*, 6, 51
- Pan, X. P., Shao, M., Colavita, M. M., Mozurkewich, D., Simon, R. S., & Johnston, K. J. 1990,
ApJ, 356, 641
- Perryman, M. A. C. 1990, in *Inertial Coordinate System on the Sky*, *IAU Symp. No. 141*,
edited by J. H. Lieske and V. K. Abalakin (Kluwer, Dordrecht), p. 297
- Press, W. H., Flannery, B. P., Teukolsky, S. A., Vetterling, W. T. 1986, *Numerical Recipes*
(Cambridge University Press, Cambridge)
- Shao, M., Colavita, M. M., Hines, B. E., Staelin, D. H., Hutter, D. J., Johnston, K. J.,
Mozurkewich, D., Simon, R. S., Hershey, J. L., Hughes, J. A., & Kaplan, G. H. 1988,

A&A, 193, 357

Shao, M., Colavita, M. M., Hines, B. E., Hershey, J. L., Hughes, J. A., Hutter, D. J.,
Kaplan, G. H., Johnston, K. J., Mozurkewich, D., Simon, R. S., & Pan, X. P. 1990,
AJ,100, 1701 (S90)

Weiler, K. W., Johnston, K. J., Mozurkewich, D., Hughes, J. A., Westerhout, G., Hutter, D. J.,
Armstrong, J. T., Simon, R. S., & Brackett, T. 1992, in High-Resolution
Imaging by Interferometry II, ESO Conference and Workshop Proceedings No. 39,
edited by J. M. Beckers and F. Merkle (ESO, Munich), p. 757

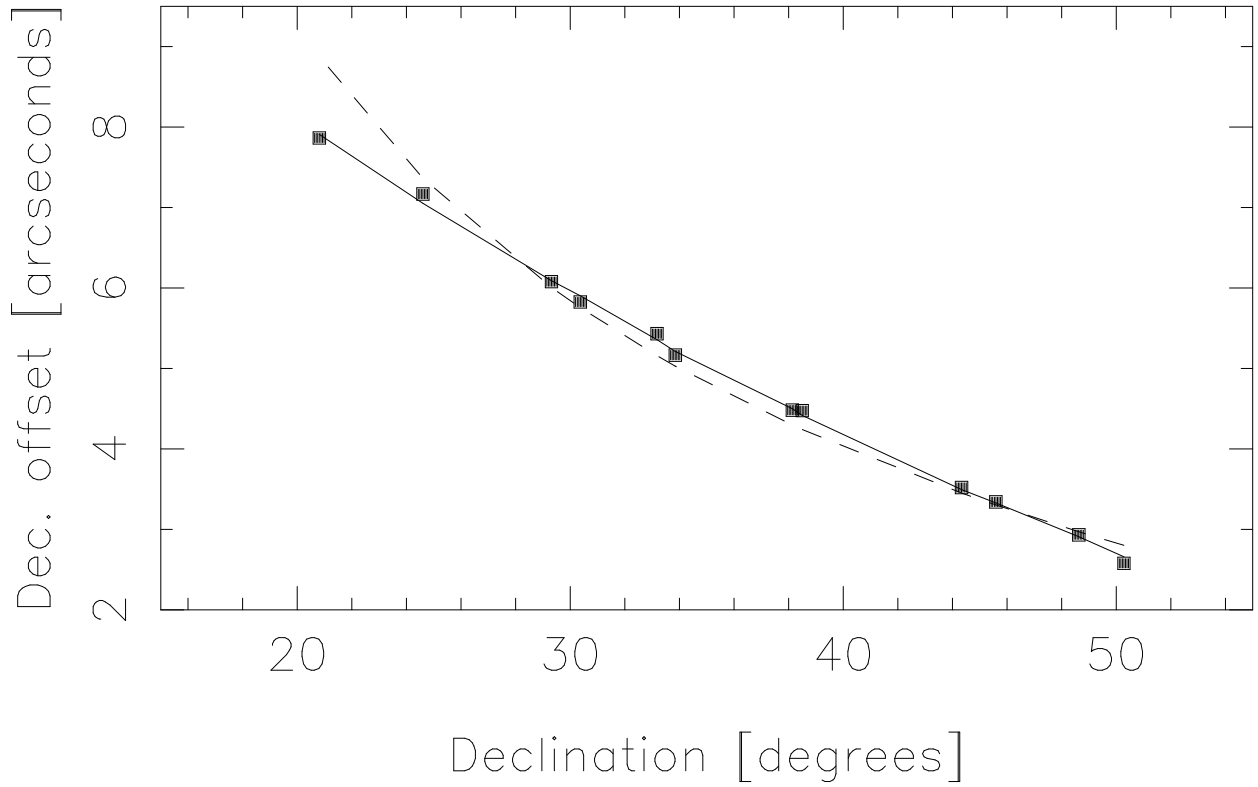


Fig. 1.— Declination offsets in August 1992 determined by a *global* solution (filled squares). Solid line connects declination offset elements (scaled) of the eigenvector; dashed line represents approximate $1/\tan \delta$ dependence on the declination δ of the star. Note that the deviations of the actual offsets from the eigenvector elements correspond to the offsets determined by the *principal* solution.

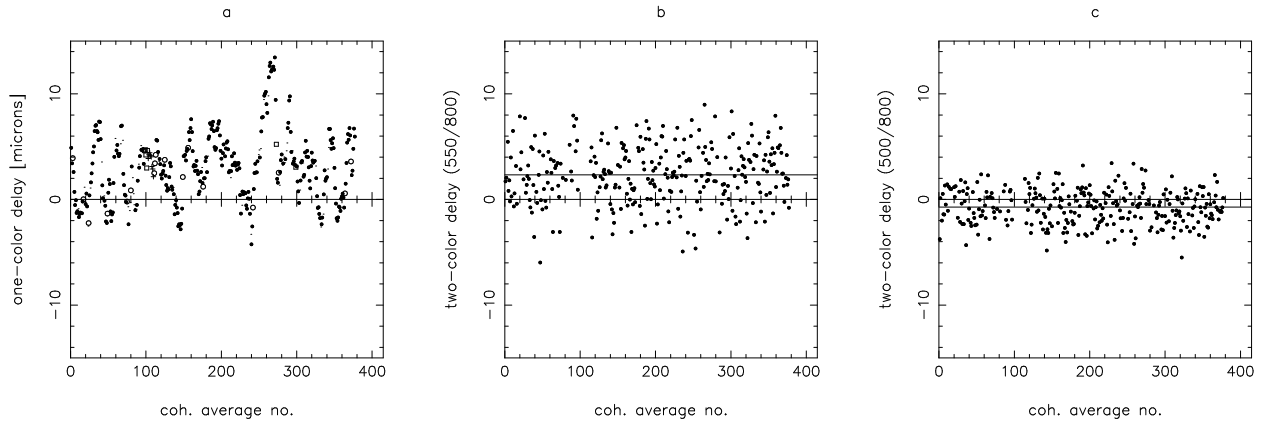


Fig. 2.— Measurements of the one-color delay in the tracking channel (a) and two-color delays (b, c) in a scan of 75 s duration. Data points are 200 ms coherent averages.

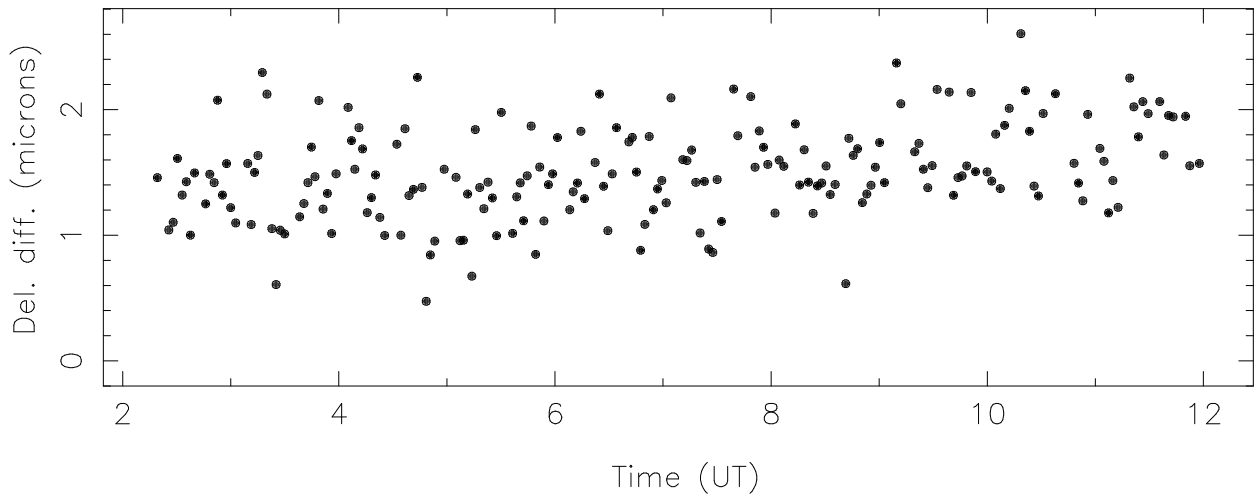


Fig. 3.— Two-color delay differences (scan-averages) between channel combinations 550/800 and 500/800.

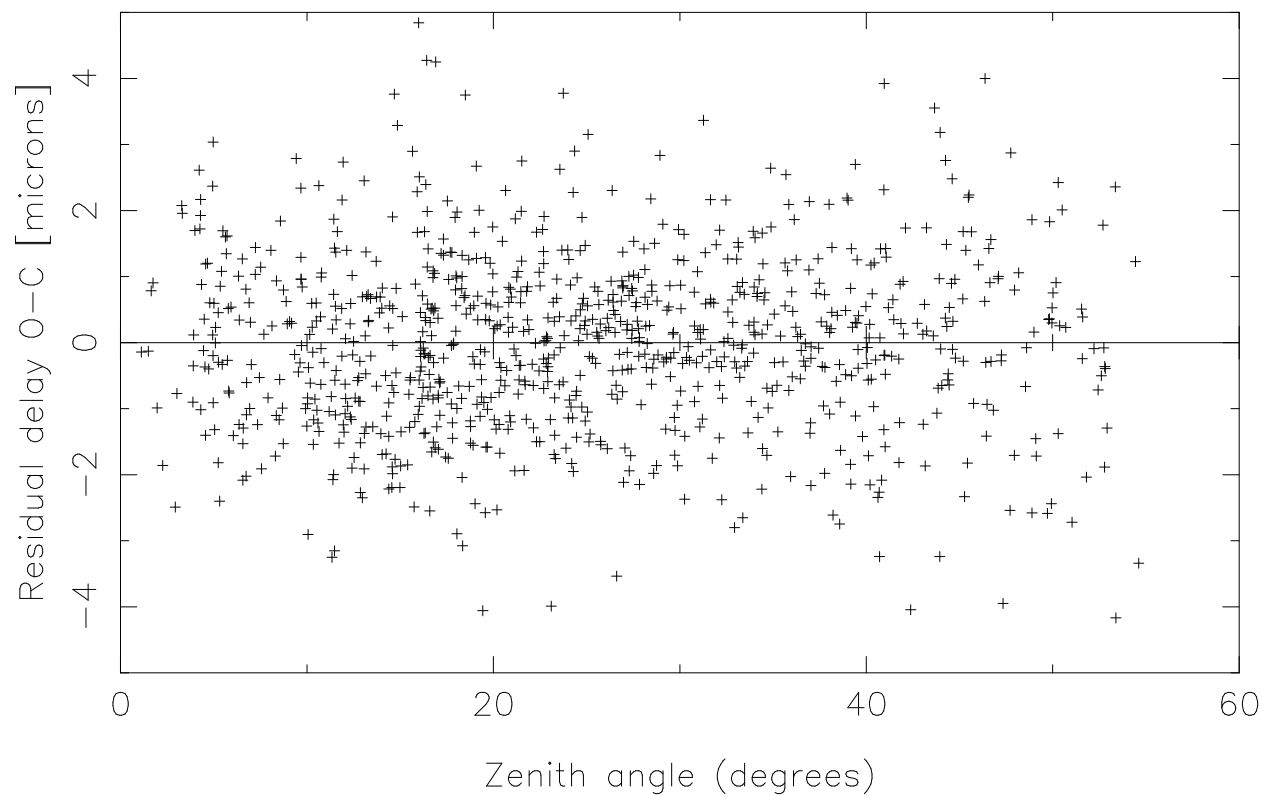


Fig. 4.— Residual delays, after fit of star positions, versus zenith angle. (Data are from the July 1989 session.)

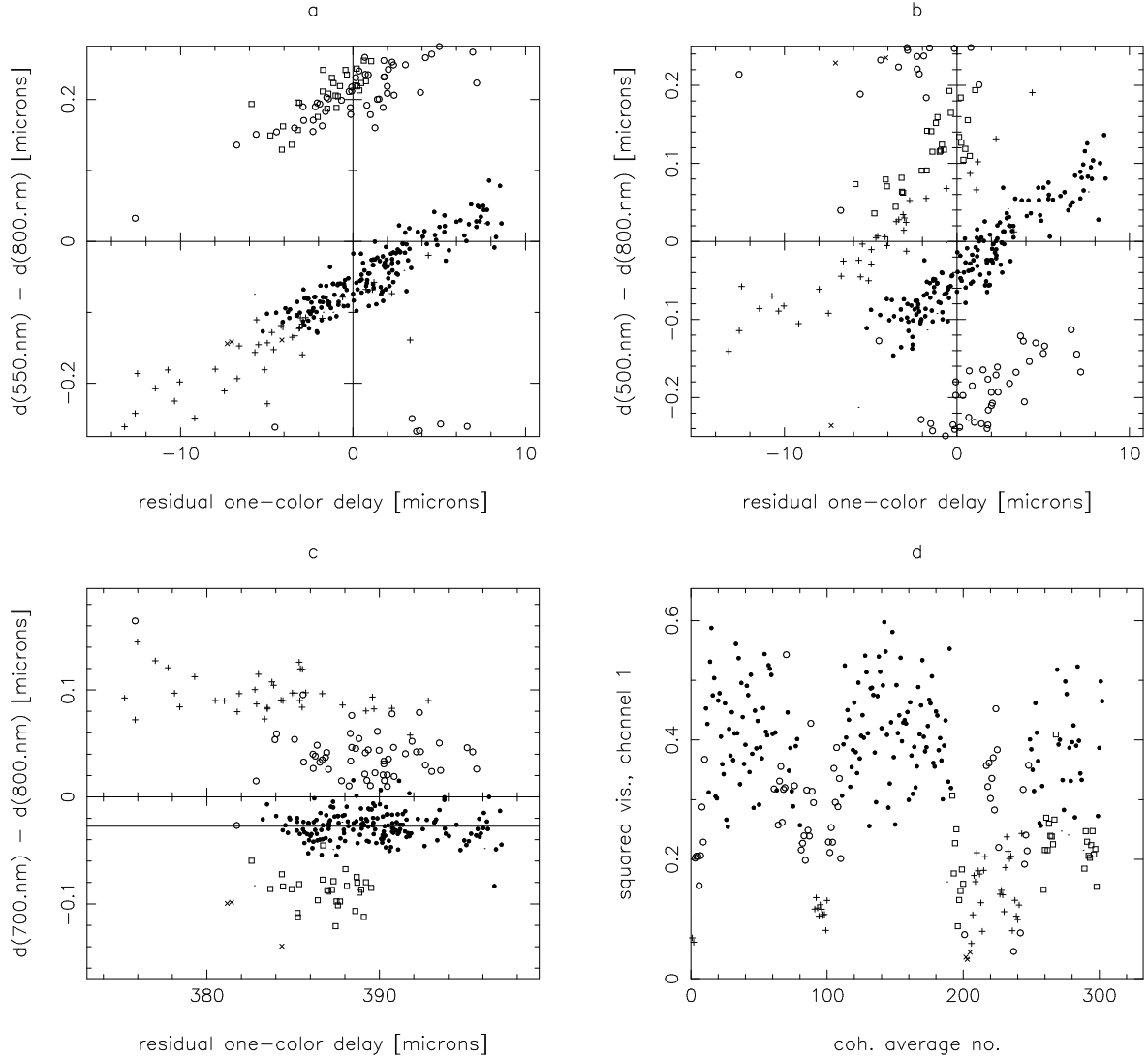


Fig. 5.— Identification of fringes. Data points (coherent averages of 200 ms, all of a single scan) are denoted by the symbols ‘plus’, ‘open circle’, ‘filled circle’, ‘open square’, and ‘cross’, according to the fringe orders -2 , -1 , 0 , $+1$, and $+2$, respectively. (Residual one-color delays in plots a and b are with respect to mean.)

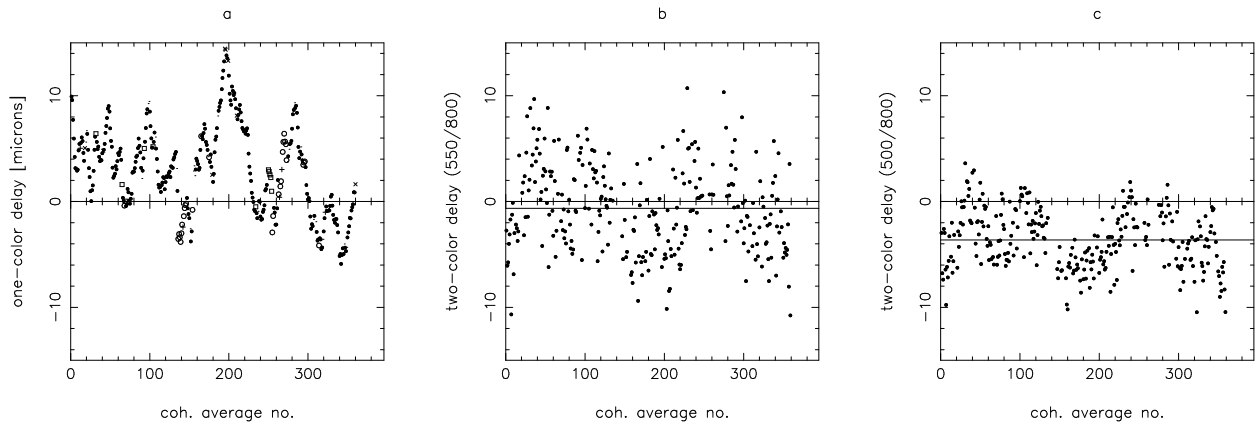


Fig. 6.— Possible effect of water vapor fluctuations on two-color delay measurements.

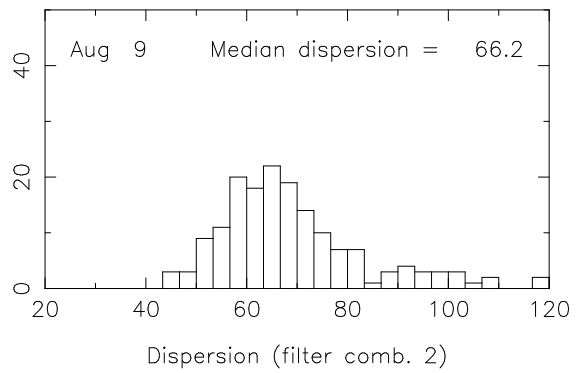
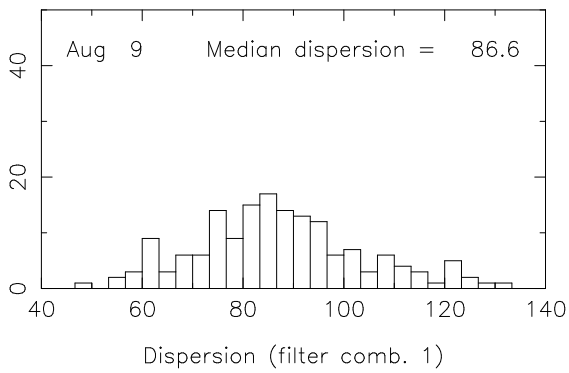
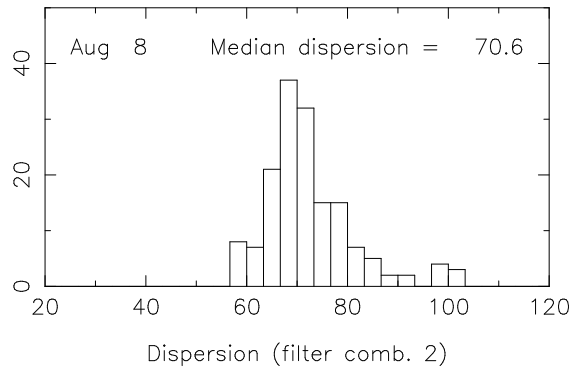
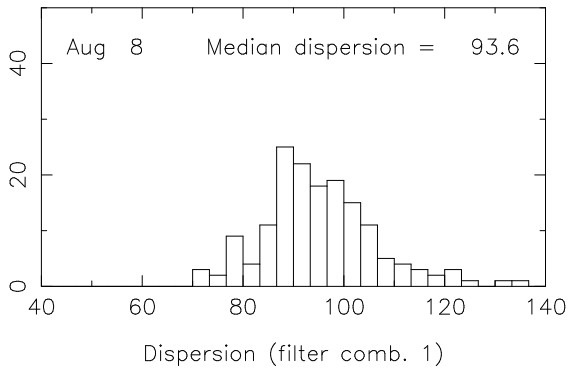
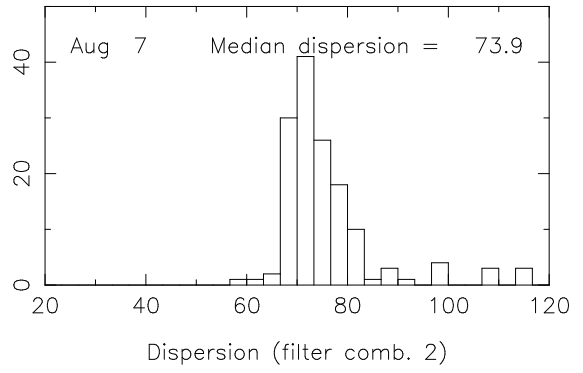
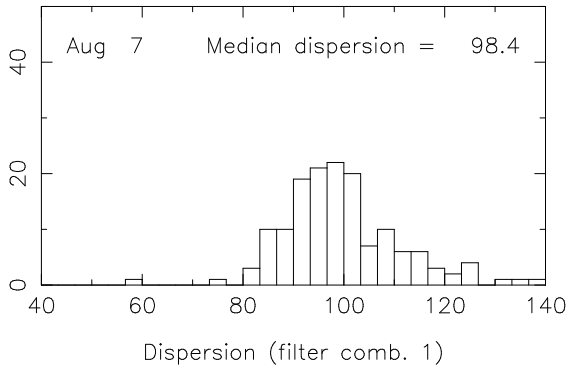


Fig. 7.— Histograms of fitted dispersion constants for three nights in August 1992.

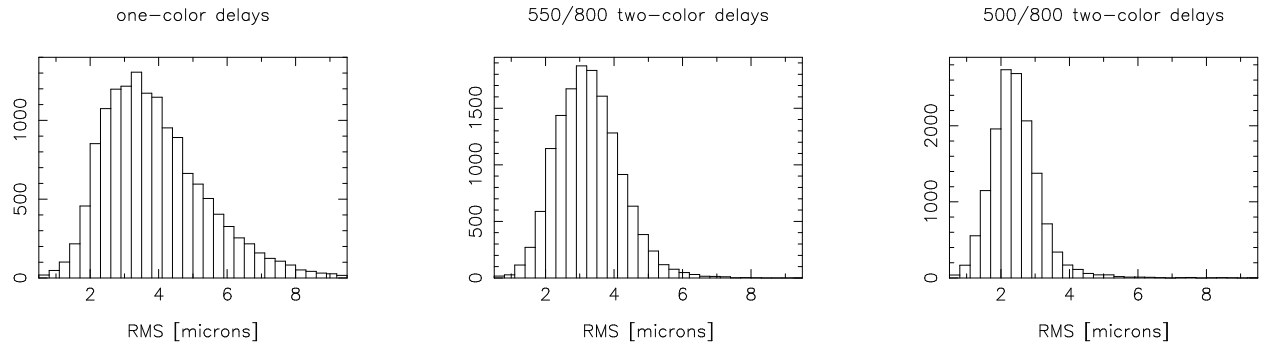


Fig. 8.— Histograms of one-color and two-color delay uncertainties.

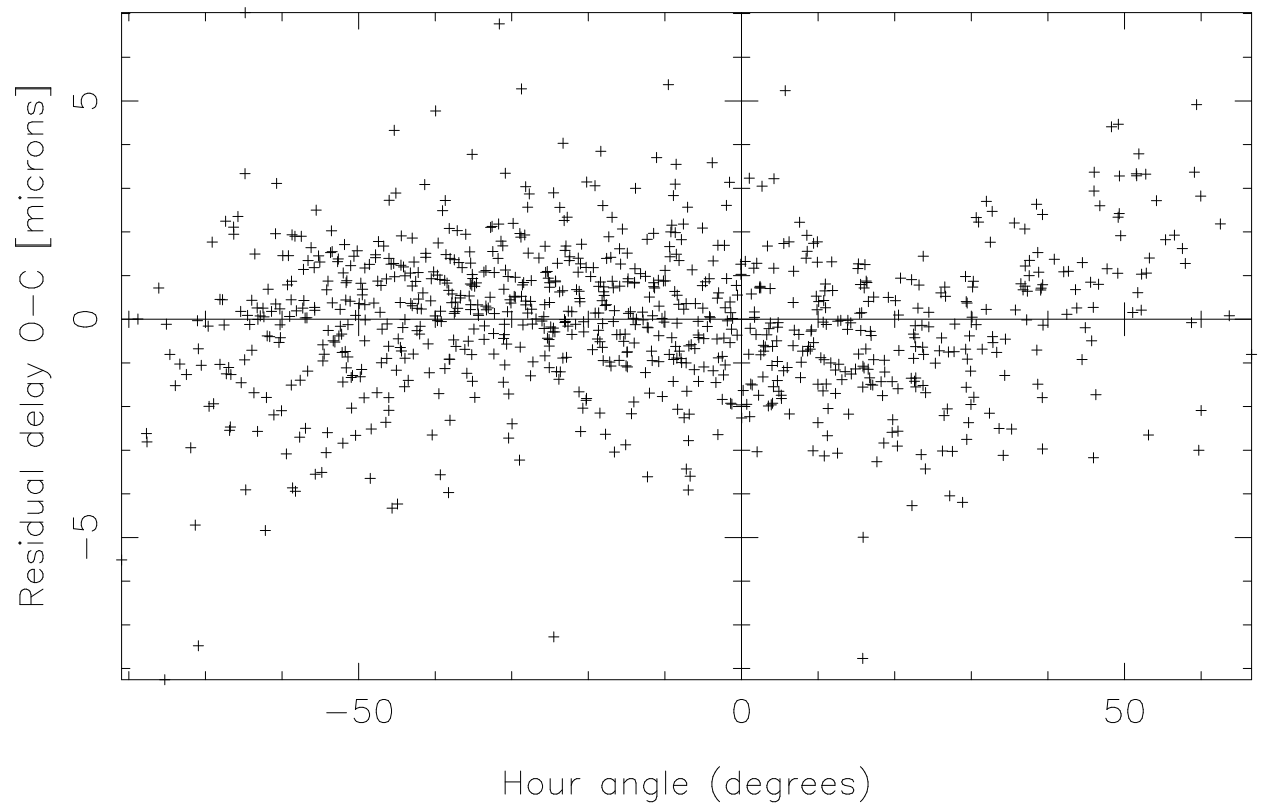
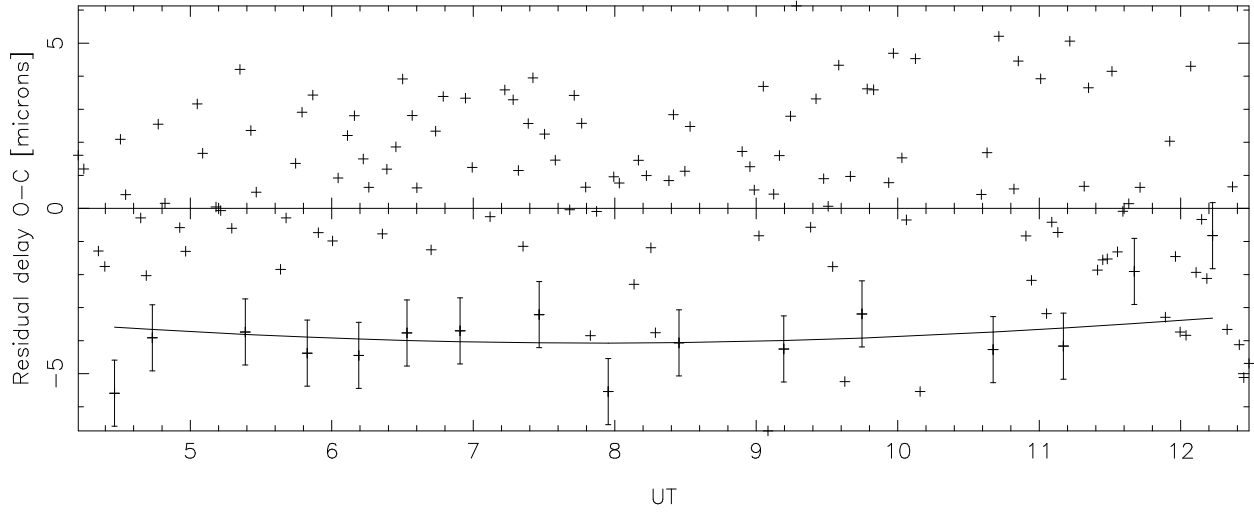
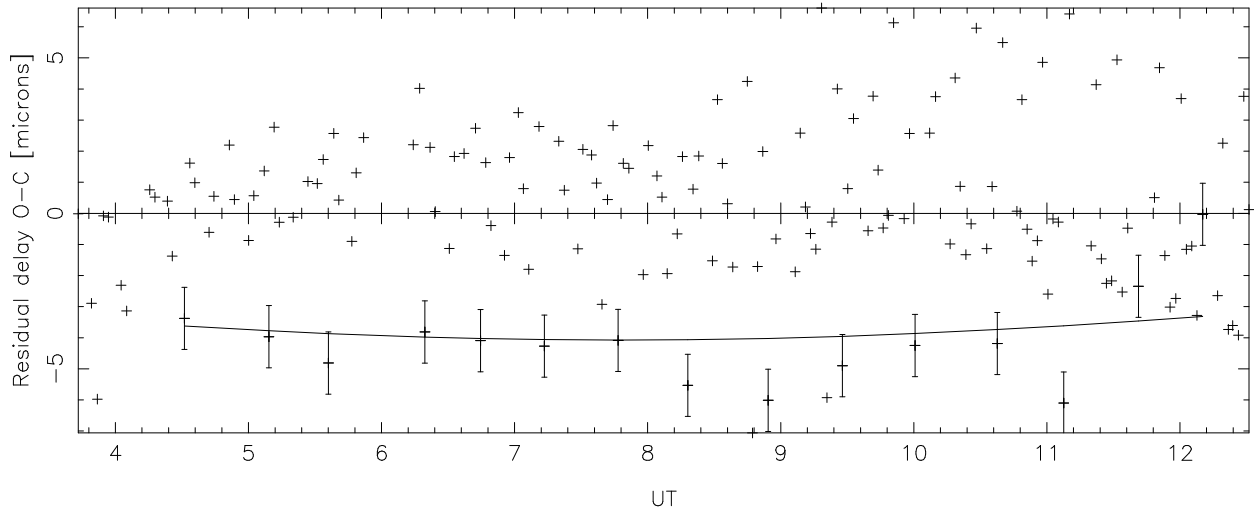


Fig. 9.— Residual delays, after fit of star positions, versus hour angle. (Data is from the August 1992 session.)

Fitted baseline 1, on 920807



Fitted baseline 1, on 920808



Fitted baseline 1, on 920809

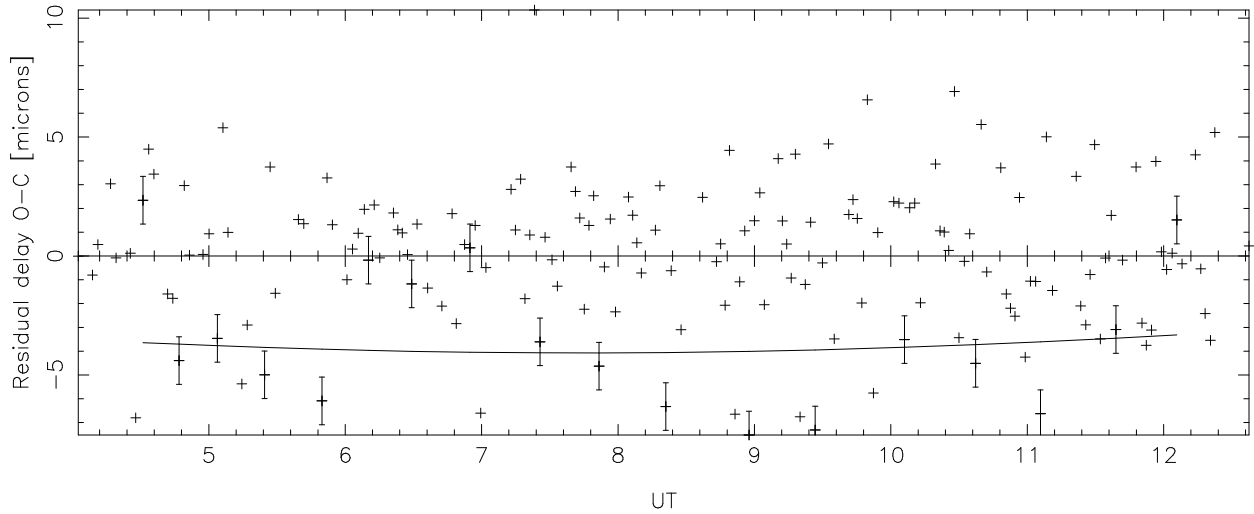


Fig. 10.— Residual delay variation of star FK5 835 (shown with uncertainties; all other stars denoted by '+'); dates: YYMMDD.

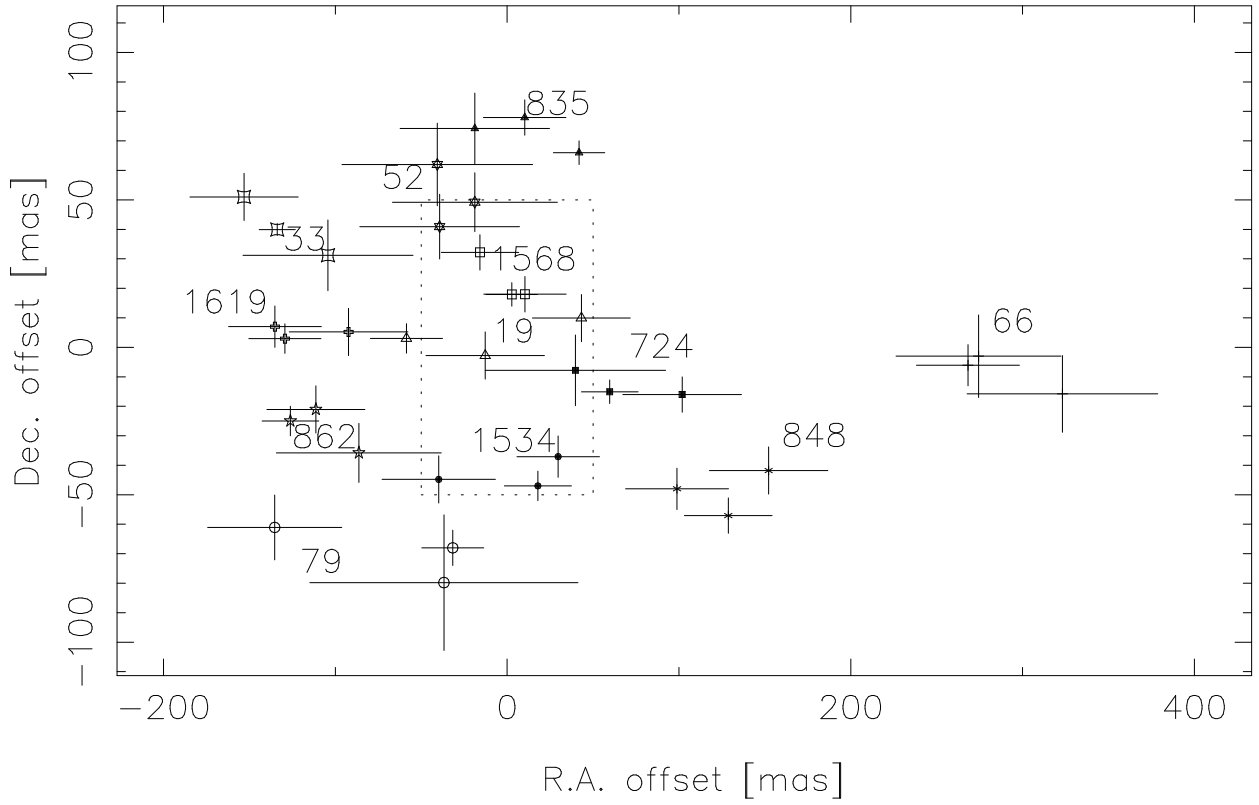


Fig. 11.— Residual positions for three nights in August 1992. Dates: see Fig. 10. A rectangular box indicates the uncertainty in the FK5 positions.

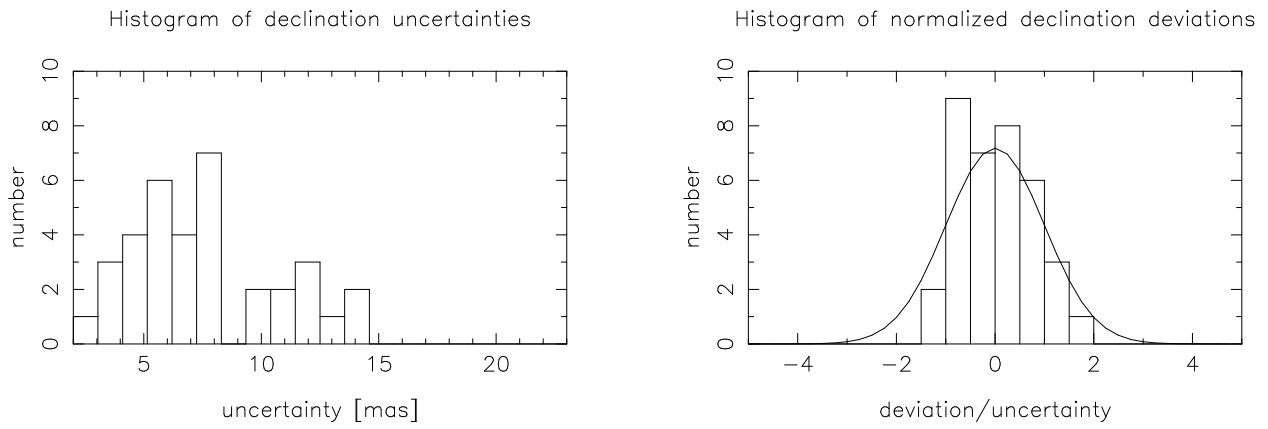


Fig. 12.— Formal uncertainties and errors of the residual positions shown in Fig. 11.

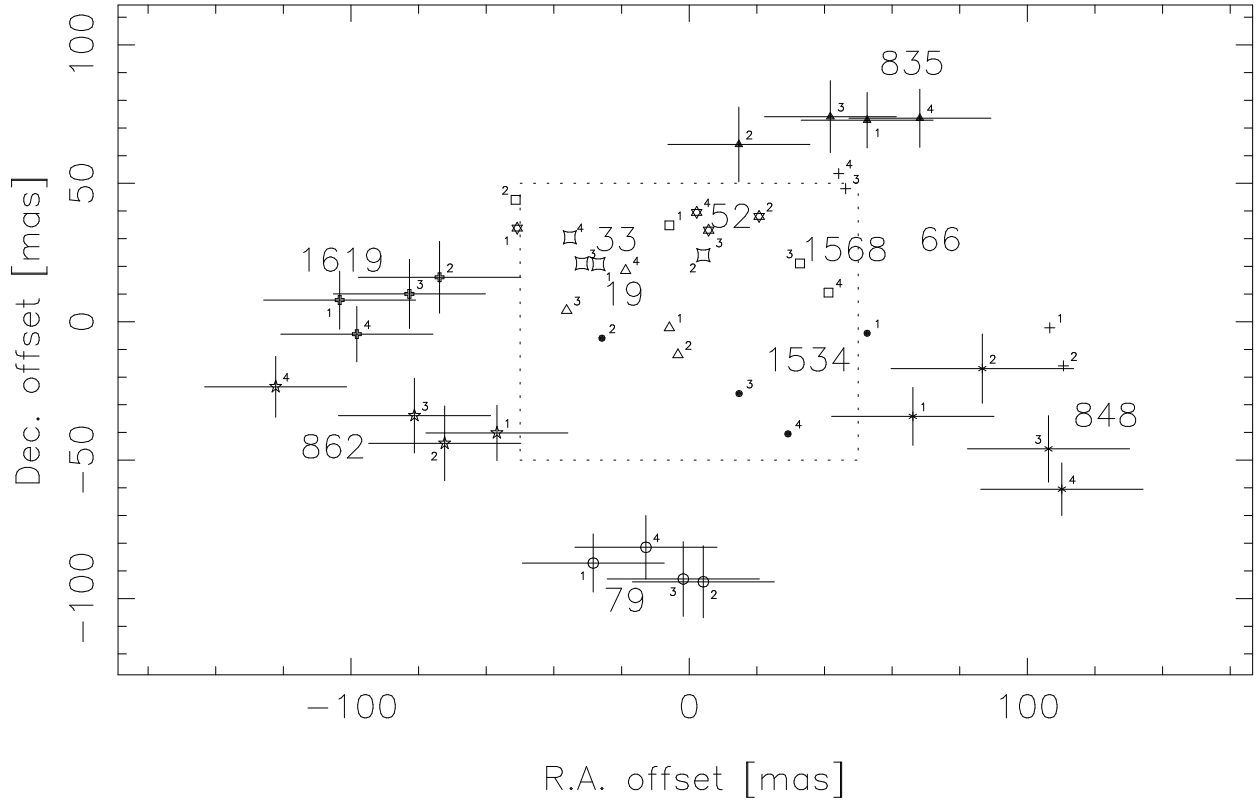


Fig. 13.— Stellar position offsets for four epochs. To avoid confusion, uncertainties have not been plotted for some of the stars. Epochs are chronologically identified with numbers 1 to 4 (see Table 2). A rectangular box indicates the uncertainty in the FK5 positions.

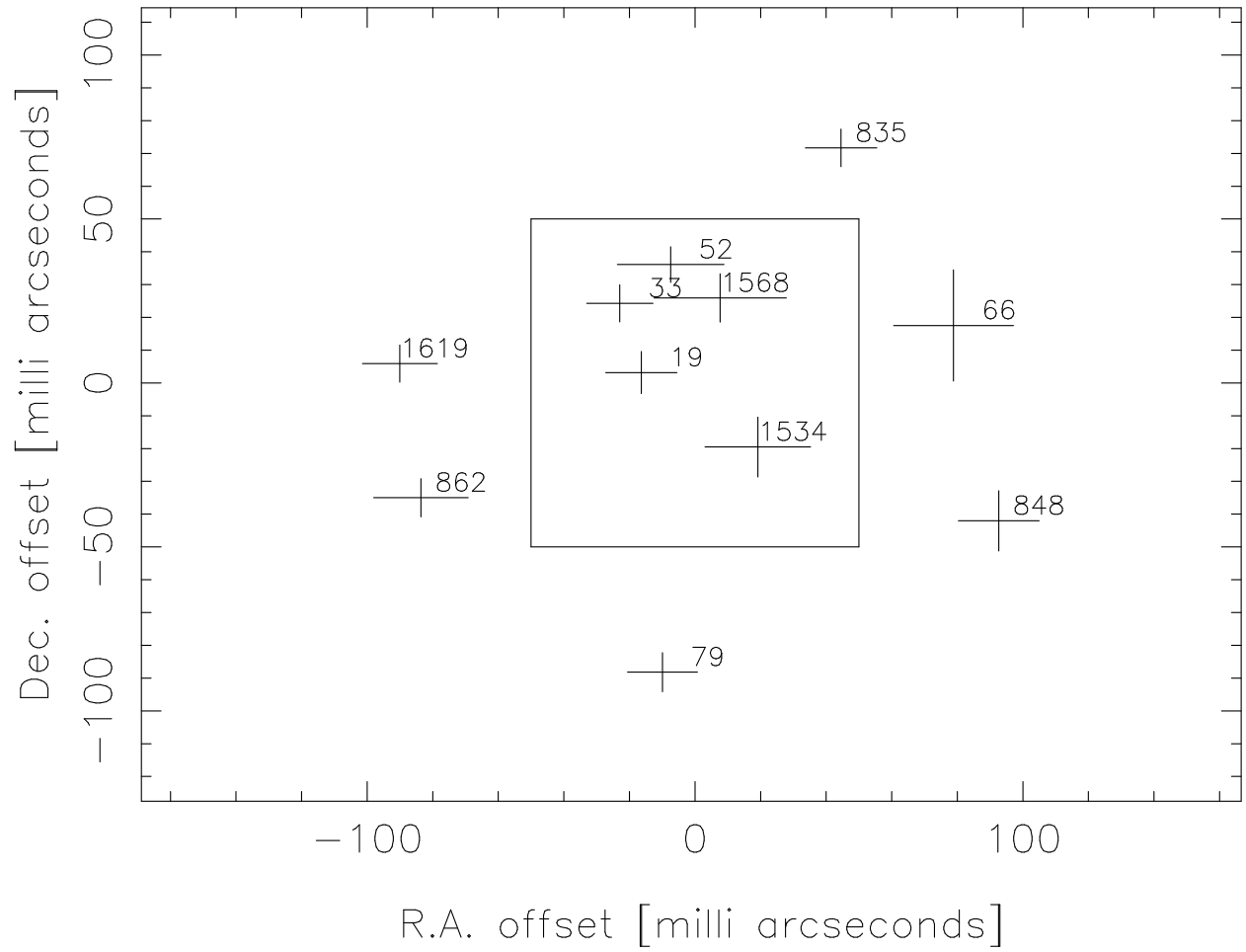


Fig. 14.— Average stellar position offsets at four epochs.

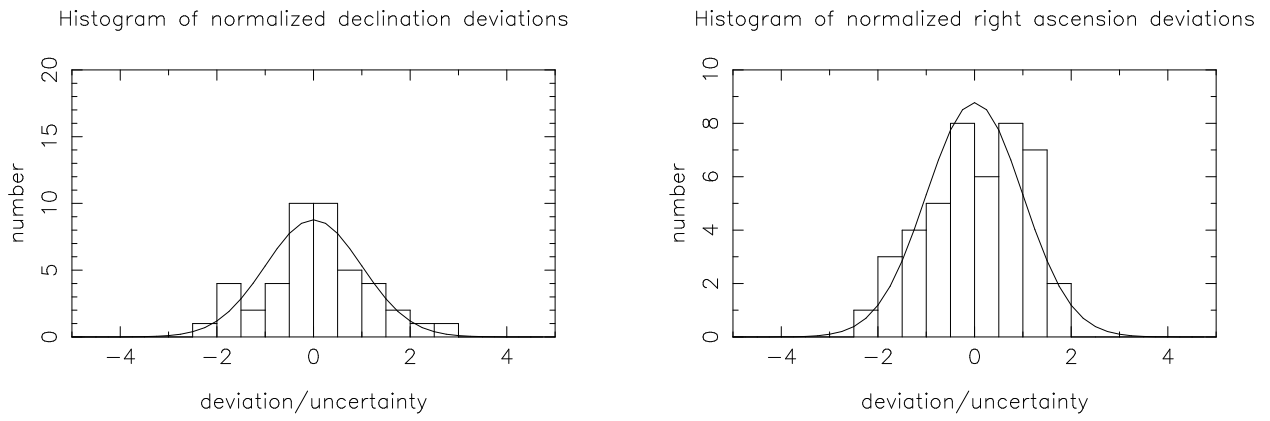


Fig. 15.— Error distribution for right ascension and declination offsets from the principal solution.

TABLE 1. List of observed stars.

FK5	Name	RA (2000)	DEC (2000)	π [mas]	μ	μ'	m_V
19	ϵ And	0 ^h 38 ^m 33 ^s .350	29°18'42".30	31	-1 ^s .739	-25".41	4 ^m 37
33	μ And	0 56 45.215	38 29 57.60	32	1.297	3.27	3 ^m 87
52	51 And	1 37 59.561	48 37 41.55	21	0.652	-11.33	3 ^m 57
66	β Ari	1 54 38.401	20 48 28.82	63	-0.684	-11.11	2 ^m 64
79	γ Tri	2 17 18.870	33 50 50.00	36	0.376	-5.12	4 ^m 01
835	π^2 Peg	22 09 59.242	33 10 41.53	7	-0.113	-2.07	4 ^m 29
848	α Lac	22 31 17.497	50 16 57.05	36	1.435	1.87	3 ^m 77
862	μ Peg	22 50 00.201	24 36 05.71	32	1.076	-4.21	3 ^m 48
1534	41 Cyg	20 29 23.736	30 22 06.84	14	0.054	0.04	4 ^m 01
1568	ρ Cyg	21 33 58.855	45 35 30.63	2	-0.218	-9.42	4 ^m 02
1619	κ And	23 40 24.519	44 20 02.18	12	0.776	-1.86	4 ^m 14

TABLE 2. Summary of observations.

Epoch	N-S nights	E-S nights
August 1988	4	4
October 1988	2	3
July 1989	4	7
August 1992	3	3

TABLE 3. Summary of results.

FK5	Name	Scans	Fit residuals [μ]		RA	\pm	DEC	\pm
	mean offset [mas]		mean	rms	[mas]	[mas]	[mas]	
1619	κ Andromedae	41	0.1	0.9	-103	22	7	10
		27	0.1	1.2	-73	23	16	13
RA	-90 \pm 11	50	0.1	1.2	-82	22	10	12
DEC	6 \pm 6	85	-0.1	1.3	-98	22	-4	10
862	μ Pegasi	56	-0.3	1.5	-56	21	-40	10
		41	0.0	1.5	-72	22	-43	13
RA	-84 \pm 14	106	-0.1	1.3	-81	22	-33	13
DEC	-35 \pm 6	66	0.0	1.8	-122	21	-23	11
79	γ Trianguli	34	-0.2	1.4	-28	21	-87	10
		45	0.0	1.4	4	21	-93	13
RA	-10 \pm 11	39	0.0	1.1	-1	22	-92	13
DEC	-88 \pm 6	50	0.0	1.3	-12	21	-81	11
52	BD+47 467	40	-0.1	1.4	-50	22	33	10
		42	-0.3	1.4	20	23	38	12
RA	-7 \pm 16	53	0.1	1.3	5	25	33	11
DEC	36 \pm 5	59	0.1	1.2	2	23	39	10
33	μ Andromedae	48	0.1	1.4	-26	19	20	10
		42	-0.1	1.4	4	21	24	13
RA	-23 \pm 10	79	0.1	1.2	-31	19	21	12
DEC	24 \pm 6	65	0.1	1.5	-35	21	30	10
19	ϵ Andromedae	47	0.0	1.1	-5	21	-2	10
		46	0.0	1.6	-3	22	-11	13
RA	-16 \pm 11	80	0.1	1.5	-36	21	4	14
DEC	3 \pm 6	62	0.3	1.4	-18	22	18	11
1568	ρ Cygni	46	0.0	1.6	-5	21	34	10
		29	0.0	1.1	-51	23	44	13
RA	8 \pm 20	122	-0.1	1.2	32	21	21	12
DEC	26 \pm 7	108	-0.1	1.4	41	21	10	10
1534	BD+29 4057	44	0.1	2.1	52	21	-4	10
		27	0.2	1.6	-25	22	-5	13
RA	19 \pm 16	125	0.0	1.5	14	21	-25	13
DEC	-20 \pm 9	85	0.1	1.9	29	21	-40	10
835	π^2 Pegasi	60	0.1	1.4	52	19	72	10
		35	0.0	1.4	14	21	64	13
RA	45 \pm 11	124	0.0	1.3	41	19	74	13
DEC	72 \pm 6	82	0.3	2.0	68	21	73	10